



Elastic Electron Scattering From Unstable Neutron-Rich ^{19}C Exotic Nucleus

R. A. Radhi, A. K. Hamoudi and A. R. Ridha*ⁱ

Department of Physics, College of Science, University of Baghdad, Baghdad, Iraq.

Abstract

The ground state proton, neutron, and matter density distributions and corresponding root-mean-square (rms) of ^{19}C exotic nucleus are studied in terms of two-frequency shell model (TFSM) approach. The single-particle wave functions of harmonic-oscillator (HO) potential are used with two different oscillator parameters b_{core} and b_{halo} . According to this model, the core nucleons of ^{18}C nucleus are assumed to move in the model space of $sp\,sd\,pf$. The shell model calculations are carried out for core nucleons with $(0 + 2)\hbar\omega$ truncations using the realistic WBP interaction. The outer (halo) neutron in ^{19}C is assumed to move in the pure $2s_{1/2}$ -orbit. The halo structure in ^{19}C is confirmed with $2s_{1/2}$ -dominant configuration. Elastic electron scattering form factor of ^{19}C nucleus is also investigated by means of the Plane Wave Born approximation. The effect of the long tail behavior (found in the calculated matter density distribution) on the elastic form factor of ^{19}C is studied. The calculated matter densities and form factors of stable ^{13}C and unstable ^{19}C are compared. It is found that the difference between the nucleon form factors of ^{13}C and ^{19}C nuclei is attributed to the difference presented in the matter densities of these nuclei. Hence the difference in the matter densities of ^{19}C and ^{13}C nuclei mainly comes from the neutron skin of the core ^{18}C and from the difference in the neutron density distribution of the last one neutron in both ^{19}C and ^{13}C nuclei. It is found that elastic electron scattering from exotic nuclei can provide predictions for the near future experiments on the electron-radioactive beam colliders where the effect of the neutron halo or skin on the charge distributions is planned to be studied.

PACS number(s): 25.60.Dz, 21.10.Gv, 27.30.+t, 13.14.Gp.

Keywords: Halo Nuclei, Two-frequency shell model, nuclear density distribution, elastic Coulomb form factor

الأستطارة الألكترونية المرنة من نواة الكربون - 19 الغريبة الغنية بالنيوترونات غير المستقرة

رعد عبد الكريم راضي، عادل خلف حمودي و أركان رفعت رضا

قسم الفيزياء، كلية العلوم، جامعة بغداد، بغداد، العراق

الخلاصة:

تم دراسة توزيعات الكثافة البروتونية والنيوترونية داخل النواة بالاضافة الى الكتلية وما يقابلها من انصاف الاقطار لنواة الكربون-19 باستخدام أنموذج القشرة ذو الترددتين. استخدمت الدوال الموجية للجسيمة

*Email: arkan_rifaah@yahoo.com

المفردة لجهد المتذبذب التوافقي مع قيمتين مختلفتين للثابت التوافقي واحدة للقلب (b_{core}) والآخرى للهالة (b_{halo}). بناء على هذا الانموذج، تم افتراض ان نيوكليونات القلب (الكاربون-18) تتحرك في فضاء $spsdpf$ ، كما وتم تنفيذ حسابات انموذج القشرة لنيوكليونات القلب مع قطع للفضاء بمقدار $(0 + 2) \hbar w$ باستخدام تفاعل WBP. نيوترون الهالة افترض بانها تسبح في المدار $2s_{1/2}$. كما وتم تحقيق عوامل التشكل المرنة لنواة الكاربون-19 بواسطة تقريب بورن للموجة المستوية. تأثير المركبة الطولية المستنتج في توزيع الكثافة الكتلي على عامل التشكل المرن للكربون-19 ايضا تم دراسته ومقارنته مع النظر المستقر الكاربون-13. وجد بان الاختلاف بين عوامل التشكل النيوكليونية للكربون-13 والكربون-19 هو يعزى الى الاختلاف الموجود في توزيعات الكثافة لهذه النوى؛ حيث ان الاختلاف في هذه التوزيعات يأتي بصورة رئيسية من الطبقة النيوترونية للقلب (الكربون-18) بالاضافة الى نيوترون الهالة الاخير في الكاربون-19. اخيرا، نتائج عوامل التشكل الكولومية المرنة للاستطارة الالكترونية المحسوبة هنا يمكن ان تزودنا بتنبؤات للتجارب المستقبلية القريبة المزمع انشاؤها في صادم الالكترون- نواة حيث يخطط فيها دراسة تأثير طبقة النيوترون او الهالة على توزيع كثافة الشحنة.

1. Introduction

Since the pioneering discovery of extraordinary enhancement in the total reaction cross section (σ_R) induced by unstable nuclei on stable targets by Tanihata et al [1], a new interesting field in nuclear physics has been turn out. An abnormally matter rms radius for neutron-rich ^{11}Li nucleus was observed much larger than other neighboring isotopes; suggesting the existence of a long tail in nuclear matter density distribution. Afterwards, this leads to the definition of neutron halo [2, 3, 4]. In addition to the measurements of σ_R , the width of momentum distribution of fragments produced by fragmentation reaction, the binding energy, the spin and parity of the ground state, and the magnetic and quadrupole moments are additional tools to confirm the halo structure in exotic nuclei.

Halo nuclei are weakly bound and spatially extended systems; they are threshold phenomenon, as the binding energy of the last nucleon(s) becomes small, the nucleon(s) becomes in the proximity of the particle continuum, the tail of the wave function extends more and more outward the central nuclear confining potential well which leads to the formation of a diffuse nuclear cloud due to quantum-mechanical penetration (the so-called nuclear halo); in turn such large diffusivity causes unusual spatial properties of the nucleon density distribution, leading to nuclear sizes deviating substantially from the $R \approx r_0 A^{1/3}$ rule. Halo nuclei are fragile and oversized, they

are expected to appear along the driplines, their structure are imagined to be composed of a tightly bound core surrounded by one or few loosely nucleons (two-nucleon halo is called Borromean [5]; where none of the binary subsystems of the core plus two-nucleons are found in bound structure). Halo nucleon(s) prefers to occupy orbits with low orbital quantum numbers, in s- or p-orbital; to lower the confining effect coming from Coulomb and centrifugal barrier which push or suppress the tail of the radial wave function toward core; leading to non-halo behaviour. The half-life time for halo nuclei are in general less than one second.

Because of the rapid decay of these nuclei, it is rather difficult to make targets with them, therefore, experiments have been done in inverse kinematics (i.e., the role of target and projectile are exchanged) with a beam of exotic nuclei incident on a stable target at radioactive ion beam (RIB) facilities.

The problem of determining the density distribution and size of halo nuclei is currently debated. The extraction of the nucleon density distribution and nuclear radius from experimental total reaction cross section of nucleus-nucleus collisions has been carried out almost exclusively by using the Glauber model in the optical-limit approximation. This is an advantage of the Glauber model that relates the cross sections of nucleus-nucleus collisions to the nuclear density and nucleon-nucleon cross sections. Experimental values obtained from such treatment are subject to controversy [6],

being sensitive to the model used to describe the reaction mechanism.

The electron scattering from nuclei is a powerful tool to investigate the electromagnetic structure in stable nuclei. This is because of the relatively weak interaction of electron with nucleus which is done through the well-known electromagnetic force. Electron scattering from exotic nuclei is not presently available; the technical proposal for the construction of electron-ion collider at GSI/Germany [7] and RIKEN/Japan facility [8] will be a great opportunity to study the electromagnetic structure of these exotic nuclei in the near future.

For one-neutron ^{19}C halo nucleus, many theoretical and experimental studies discussed and confirmed the halo structure in [9 - 19].

The no-core shell model (NCSM) calculations in light nuclei were applied to halo nuclei with poor agreement [20-23] for rms radii and separation energies compared with experimental data even for large model space. This is probably related to the Gaussian fall-off of the NCSM wave functions, which does not reproduce the correct exponential tail. The limitation of no-core shell model is arising from the increasing dimensionality with mass for a given model space, therefore, It will be a very cumbersome and time consuming.

The two-frequency shell-model (TFSM) approach was employed successfully on halo nuclei [24, 25], for both valence energy and rms radii. Within this model, one uses harmonic-oscillator (HO) wave functions with two oscillator size parameters, b_{core} and b_{halo} for the core and halo orbits, respectively. This technique will enable one to work freely on each part by changing $b_{core(halo)}$ till one can get a fit with some experimental results.

Unfortunately there is no application of the TFSM approach on nucleon densities and elastic electron form factors for exotic nuclei. For this reason, we undertake the studying of such substantial quantities for halo ^{19}C nucleus in such approach. The elastic electron scattering form factors in this work are calculated in plane-wave Born approximation (PWBA) through matter densities obtained from the TFSM calculations. The effect of the long tail component observed in the calculated nucleon densities on elastic electron form factors for ^{19}C

nucleus is discussed. Besides, the matter rms radii are also calculated according to this model.

2. Theory

The one-body operator of rank ΔJ of the longitudinal transition density for point protons (with isospin $t_z = 1/2$) or neutrons ($t_z = -1/2$) is given by [26]:

$$\hat{\rho}_{\Delta J, t_z}^L = \sum_{k=1}^A e(t_z) \frac{\delta(r - r_k)}{r_k^2} Y_{\Delta J, M_{\Delta J}}(\Omega_{r_k}), \quad (1)$$

with

$$e(t_z) = \frac{1 + 2t_z(k)}{2}.$$

In Eq. (1), the superscript (L) in the operator $\hat{\rho}_{\Delta J, t_z}^L$, stands for longitudinal component, $Y_{\Delta J, M_{\Delta J}}(\Omega_{r_k})$ and $\delta(r - r_k)$ are the spherical harmonic and Dirac delta functions, respectively.

The reduced matrix element of the longitudinal transition density operator, in Eq. (1), can be expressed as [26]:

$$\langle J_f \| \hat{\rho}_{\Delta J, t_z}^L(\vec{r}) \| J_i \rangle = \frac{1}{\sqrt{4\pi(2J_i + 1)}} \times$$

$$\sum_{ab} OBDM(J_f, J_i, \Delta J, a, b, t_z) \langle j_a \| Y_{\Delta J} \| j_b \rangle \times R_{n_a l_a}(r) R_{n_b l_b}(r) \quad (2)$$

where a and b label single-particle states for the considered shell model space and are specified by:

$$|p\rangle = |n_p l_p\rangle |j_p m_p\rangle,$$

(the state p represents either a or b).

The states $|J_i\rangle$ and $|J_f\rangle$ are characterized by the model space wave functions. In Eq. (2), $R_{n_p l_p}(r)$ is the radial part of the harmonic oscillator wave function, $\langle j_a \| Y_{\Delta J} \| j_b \rangle$ is the reduced matrix element of the spherical harmonic and $OBDM(J_f, J_i, \Delta J, a, b, t_z)$ is the proton ($t_z = 1/2$) or neutron ($t_z = -1/2$) one-body density matrix element given by the second quantization notation as [26]:

$$OBDM(J_f, J_i, \Delta J, a, b, t_z) = \frac{\langle J_f \parallel [a_{a,t_z}^+ \otimes \tilde{a}_{b,t_z}]^{\Delta J} \parallel J_i \rangle}{\sqrt{2\Delta J + 1}} \dots\dots(3)$$

As the *spsdpf*- shell wave functions (generated in the present study with WBP interactions [27]), have good isospin, it is appropriate to evaluate the *OBDM* elements by means of isospin-reduced matrix elements. The relation between these tripled-reduced *OBDM* and the proton or neutron *OBDM* of Eq. (2) is given by [28]:

$$OBDM(t_z) = (-1)^{T_f - T_z} \sqrt{2} \begin{pmatrix} T_f & 0 & T_i \\ -T_z & 0 & T_z \end{pmatrix} \\ \times OBDM(\Delta T = 0) / 2 + 2t_z (-1)^{T_f - T_z} \sqrt{6} \begin{pmatrix} T_f & 1 & T_i \\ -T_z & 0 & T_z \end{pmatrix} \\ \times OBDM(\Delta T = 1) / 2. \dots\dots\dots(4)$$

The tripled-reduced *OBDM*(ΔT) elements are given in terms of the second quantization notation as:

$$OBDM(i, f, \Delta J, \alpha, \beta, \Delta T) = \frac{\langle \Gamma_f \parallel [a_{\alpha}^+ \otimes \tilde{a}_{\beta}]^{\Delta J, \Delta T} \parallel \Gamma_i \rangle}{\sqrt{2\Delta J + 1} \sqrt{2\Delta T + 1}} \dots\dots\dots(5)$$

Here, Greek symbols are utilized to indicate quantum numbers in coordinate space and isospace (i.e., $\Gamma_i \equiv J_i T_i$ and $\Gamma_f \equiv J_f T_f$).

The *OBDM*(ΔT) elements contain all the information about transitions of a given multipolarities which are embedded in the model wave functions. To obtain these *OBDM* elements, shell model calculations are performed using WBP interaction for the core nucleons of ¹⁹C nucleus.

For the ground state density distribution, we have $J_i = J_f$, $\Delta J = 0$, then Eq. (2) reduces to the following:

$$\rho_{t_z}(r) = \frac{1}{\sqrt{4\pi(2J_i + 1)}} \sum_{ab} OBDM(J_i, J_i, 0, a, b, t_z) \\ \times \langle j_a \parallel Y_0 \parallel j_b \rangle R_{n_a l_a}(r) R_{n_b l_b}(r). \quad (6)$$

Where

$$\rho_{t_z}(r) = \langle J_i \parallel \hat{\rho}_{\Delta J=0, t_z}^L(\vec{r}) \parallel J_i \rangle.$$

As halo nuclei, are oversized and easily broken systems consisting of a compact core plus a number of outer nucleons loosely bound and spatially extended far from the core, it is suitable to separate the ground state density distribution of Eq. (6) into two parts. The first part is connected to the core nucleons while the second part is connected to the halo (outer) nucleons, i.e.:

$$\rho_m(r) = \rho^{core}(r) + \rho^{halo}(r). \quad (7)$$

where the subscript (m) in Eq. (7) denotes matter.

Moreover, Eq. (6) may also be expressed as:

$$\rho_m(r) = \rho_p(r) + \rho_n(r), \quad (8)$$

where $\rho_p(r)$ and $\rho_n(r)$ are the ground state proton and neutron densities of halo nuclei and expressed as:

$$\rho_p(r) = \rho_p^{core}(r) + \rho_p^{halo}(r) \quad (9)$$

and

$$\rho_n(r) = \rho_n^{core}(r) + \rho_n^{halo}(r). \quad (10)$$

The normalization condition of the above ground state densities is given by:

$$g = 4\pi \int_0^{\infty} \rho^g(r) r^2 dr. \quad (11)$$

Here, $\rho^g(r)$ represents one of the following densities: $\rho_m(r)$, $\rho^{core}(r)$, $\rho^{halo}(r)$, $\rho_p(r)$, $\rho_n(r)$. In that case, the parameter *g* represents, correspondingly, one of the following quantities: the nuclear mass (*A*), the number of core nucleons, the number of halo nucleons, the total number of protons and the total number of neutrons of halo nuclei. The rms radii of corresponding above densities are given by:

$$\langle r^2 \rangle_g^{1/2} = \frac{4\pi}{g} \int_0^{\infty} \rho^g(r) r^4 dr. \quad (12)$$

The plane wave Born approximation (PWBA) is used to study the elastic electron

scattering form factors from considered nuclei. In the PWBA, the incident and scattered electron waves are represented by plane waves. The elastic proton form factor is simply given by the Fourier-Bessel transform of the ground state proton density distribution, i.e.

$$F(q) = \frac{4\pi}{Z} \int_0^{\infty} \rho_p(r) j_0(qr) r^2 dr \quad (13)$$

where $j_0(qr)$ is the spherical Bessel function of order zero and q is the momentum transfer from the incident electron to the target nucleus.

In the limit $q \rightarrow 0$, the target nucleus will be characterized as a point particle. Accordingly, using Eq. (13) with the help of Eq. (9), the proton form factor of this target nucleus will be equal to unity (i.e. $F(q \rightarrow 0) = 1$).

3. Results and discussion

The TFSM approach [24, 25] is employed to study the ground state proton, neutron and matter densities, the proton, neutron and matter rms radii and elastic nucleon form factors of unstable ^{19}C halo nucleus. The single particle harmonic oscillator wave functions are used with two different oscillator size parameters b_{core} and b_{halo} . To obtain the one body density matrix (OBDM) elements of the core and halo parts, we perform shell model calculations via the computer code OXBASH [29].

^{19}C is a one-neutron halo nucleus ($J^\pi T = \frac{1}{2}^+ \frac{7}{2}$) composed of the core ^{18}C nucleus ($J^\pi T = 0^+ 3$) plus one loosely bound neutron surrounding the core; the one-neutron halo is considered to be in $2s_{1/2}$ orbit. The separation energy of the outer (halo) neutron is $S_{1n} = 0.16(11)$ MeV [9, 30]. The oscillator size parameter b_{core} is chosen to be 1.785 fm, to reproduce the experimental matter rms radius of the core ^{18}C . The calculated matter rms radius of core ^{18}C for such chosen b_{core} is 2.822 fm which is in good agreement with experimental value, 2.82 ± 0.04 fm [9]. While that for the outer (halo) neutron b_{halo} is taken to be 3.53 fm to reproduce the experimental matter rms radius of ^{19}C nucleus. Adopting these values of b_{core} and b_{halo} , the calculated neutron, proton, and matter rms radii are 3.340, 2.627, and 3.133 fm, respectively. It is so clear that the calculated

matter rms radius is in excellent agreement with experimental value (3.13 ± 0.07 fm) [10]. The difference between the calculated overall neutron and proton rms radii is 0.713 fm. This difference indicates a halo structure in ^{19}C nucleus.

The matter density $\rho_m(r)$ (in fm^{-3}) of ^{19}C is plotted in figure 1 as a function of r (in fm). In this figure, we assume that the core nucleons of ^{18}C move within the *spsdpf* – model space. The one body density matrix (OBDM) elements of such model space wave functions are obtained by performing shell model calculations of ^{18}C nucleus using the realistic WBP interaction [27] with $(0+2)\hbar\omega$ truncations.

In figure 1 we assume that the outer neutron in ^{19}C moves in the pure $2s_{1/2}$ (denoted by the solid curve). The experimental data of matter densities (denoted by filled circles) [9] are (deduced from the Glauber model) displayed in this figure for comparison. It is so clear from figure 1 that the solid curve is in good agreement with the experimental data up to 5.8 fm and beyond that it oscillates around the data. The long tail behavior, which is a distinguishing signal of halo nuclei, is markedly exposed in the solid curve.

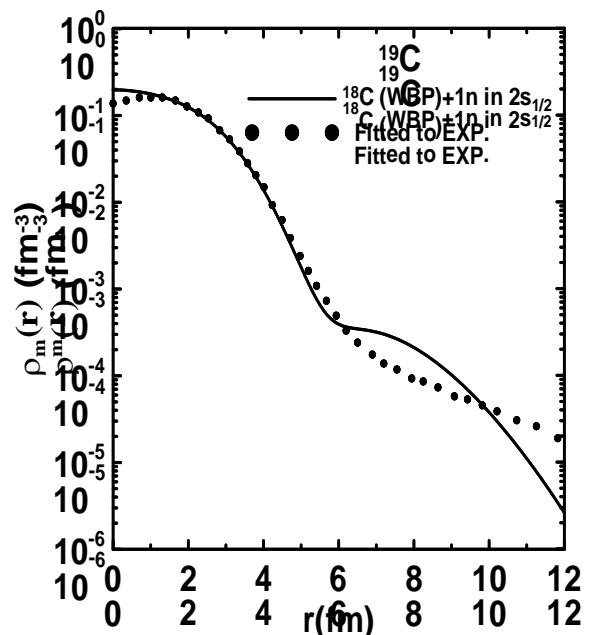


Figure 1-The calculated matter densities of ^{19}C halo nucleus. The dotted line represents the experimental data extracted from Glauber model [9].

In figure 2, the calculations are repeated exactly as in figure 1, but this time for the proton $\rho_p(r)$ and neutron $\rho_n(r)$ density distributions of ^{19}C . The solid curve is the calculated neutron density of ^{19}C when the outer (halo) neutron moves in the pure $2s_{1/2}$ -orbit while the plus distribution is the calculated proton density. The long tail behavior (which is a characteristic mark of halo nuclei) is noticeably seen in the neutron distribution. This behavior is related to the existence of the outer neutron of ^{19}C in the halo $2s_{1/2}$ -orbit.

The calculated proton density of ^{19}C shown in figure 2 demonstrates a steep slope behavior because there are no protons found in the halo orbits (all protons of ^{19}C are found within their core only). It is useful to remark that the halo phenomenon in ^{19}C is connected to the matter and neutron densities and not to the proton density.

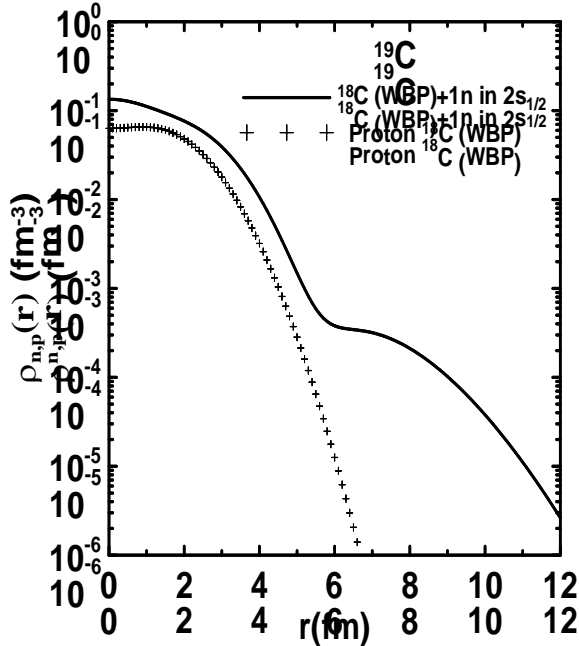


Figure 2- The calculated proton and neutron densities of ^{19}C exotic nucleus.

In figure 3, the matter densities of unstable ^{19}C and stable isotope ^{13}C are displayed by the solid and dash-dotted curves, respectively. The matter density of unstable ^{19}C is that calculated in figure 2. The matter distribution of stable ^{13}C shown in figure 3 is calculated by means of the WBP interaction, where all nucleons of ^{13}C are considered to move within the configurations of the $spsdpf$ - space with $(0+2)\hbar\omega$ truncations.

It is so clear from figure 3 that the matter density distributions of ^{19}C and ^{13}C nuclei are diverse. As the outer (halo) neutron in ^{19}C is weakly bound, the matter density distribution of ^{19}C has a longer tail than that of ^{13}C nucleus. This can be seen obviously from the comparison between the matter density distributions of ^{19}C and ^{13}C shown in figure 3.

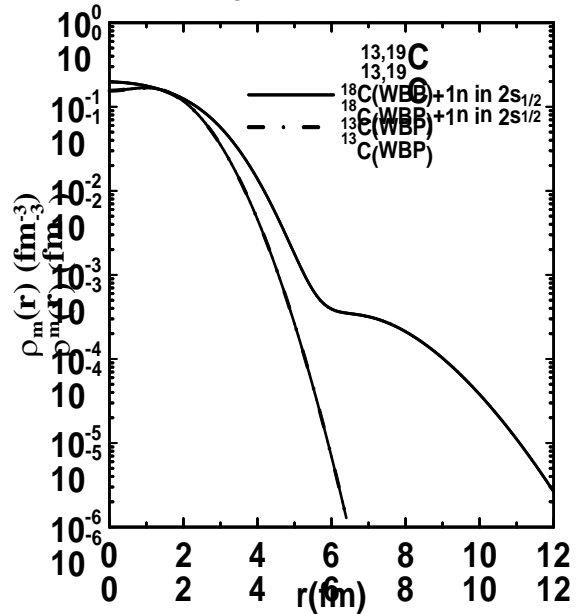


Figure 3-The calculated matter densities for halo ^{19}C compared with that of stable ^{13}C

To seek out if the long tail behavior of the matter density distribution of the neutron-rich nuclei demonstrates noticeable effects in the process of elastic electron scattering, elastic nucleon form factors for unstable neutron-rich ^{19}C and stable ^{13}C are calculated by means of the Plane Wave Born Approximation (PWBA).

In figure 4, the dependence of the squared nucleon form factor $|F(q)|^2$ on the momentum transfer q (in fm^{-1}) is exhibited, where the input matter density distributions are those of figure 3. The calculated form factors of the stable ^{13}C and unstable ^{19}C nuclei are displayed by the dash-dotted and solid curves, respectively. The experimental elastic charge form factors of stable ^{13}C [30] are displayed by open circles for comparison. Figure 4 illustrates that both the behavior and the magnitude of the calculated nucleon form factors (the dash-dotted curve) of ^{13}C are in good agreement with all experimental data with slight deviation around the first observable diffraction minimum, where the available data for ^{13}C cover only the range of

$q \leq 3.5 \text{ fm}^{-1}$. However, this comparison gives the conclusion that the PWBA can reproduce the experimental data of elastic electron scattering on the stable ^{13}C . The elastic electron scattering form factors of unstable neutron-rich ^{19}C nucleus can be also discussed. It is so apparent from figure 4 that the calculated nucleon form factors of unstable ^{19}C (the solid curve) has two diffraction minima (located at momentum transfer $q = 1.6$ and $q = 2.6 \text{ fm}^{-1}$) and two diffraction maxima (located at $q = 1.9$ and $q = 2.88 \text{ fm}^{-1}$) whereas that of stable ^{13}C (the dash-dotted curve) has one diffraction minimum (located at $q = 1.75 \text{ fm}^{-1}$) and one diffraction maximum (located at $q = 2.1 \text{ fm}^{-1}$). The positions of the first and second diffraction minima of ^{19}C have inward and outward shifts of approximately 0.15 and 0.85 fm^{-1} , respectively as compared with the first observable diffraction minimum of ^{13}C .

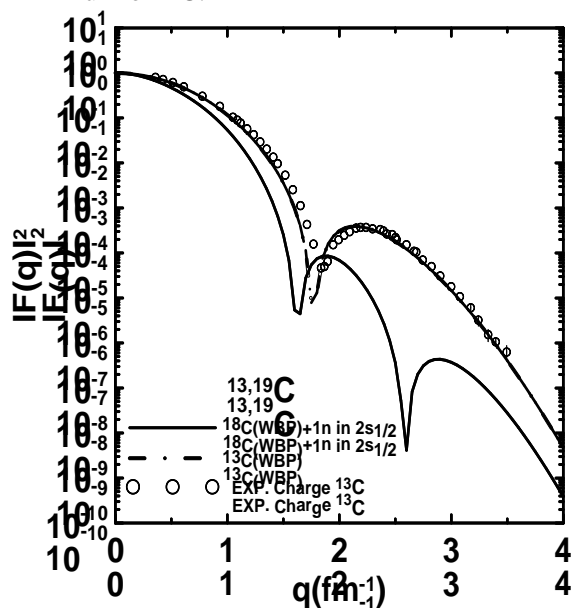


Figure 4-The calculated nucleon form factors for halo ^{19}C compared with that calculated for stable ^{13}C . The open circles represent the experimental charge form factor for ^{13}C [31].

As mentioned before, the elastic nucleon form factor in the nucleus is simply connected to its matter density distribution. For that reason, the difference between the nucleon form factors of ^{19}C and that of ^{13}C is owing to the different matter density distributions of the two nuclei. The difference between the matter density distributions of ^{19}C and ^{13}C is essentially caused by two reasons; the first is due to the effect of

the neutron skin of the core ^{18}C and the second is due to the difference in the neutron density distribution of the last neutron in both ^{19}C and ^{13}C nuclei.

To analyze the effect of the long tail of the matter density distribution on elastic electron-nucleus scattering, one requires identifying which part of the form factor is responsive to the tail of the matter density. It is recognized from the fitting to the experimental data of ^{12}C [31] and ^{32}S [32] that the form factors in the region of momentum transfer $1 \leq q \leq 3 \text{ fm}^{-1}$ are responsive to the change of the tail part of the density distribution, whereas those at the region of high momentum transfer $q \geq 3 \text{ fm}^{-1}$ are responsive to the change of the central part of the density distribution. It is expected that the conclusions of ^{12}C [31] and ^{32}S [32] work as well for C isotopes. Therefore, one may attribute the difference of the calculated form factors at $1 \leq q \leq 3 \text{ fm}^{-1}$ between ^{19}C and ^{13}C (figure 4) to the influence of the long tail of the neutron density distributions of ^{19}C while that at $q \geq 3 \text{ fm}^{-1}$ to the influence of the neutron density differences at the central parts.

4. Conclusions

The long tail behavior, considered as a distinctive feature of halo nuclei, is evidently revealed in the calculated neutron and matter density distributions. Besides, the noticeable difference that is found between the calculated overall proton and neutron rms radii of ^{19}C also indicates a halo structure. It is found that the structure of ^{19}C has $2s_{1/2}$ -dominant configuration. The difference observed between the nucleon form factors of ^{19}C and ^{13}C is generally caused by the difference in the matter density distribution resulting from the existing of the neutron skin in the core of ^{18}C and from the difference in the neutron densities of the last neutron in ^{19}C and ^{13}C . Moreover, the difference between the nucleon and proton form factor of the above unstable and stable isotope at the region $1 \leq q \leq 3 \text{ fm}^{-1}$ is mainly caused by the influence of the long tail behavior presented in the neutron density distribution, while that at the region of $q \geq 3 \text{ fm}^{-1}$ to the influence of the neutron density difference at the central parts.

Because the difference of the nucleon form factors between the stable nucleus and its neutron drip-line isotope has observable effects, we regard that elastic electron scattering is an efficient tool to examine neutron-halo phenomena in neutron-rich nuclei.

Acknowledgment

The authors would like to express their thanks to Professor B. A. Brown of the National Superconducting Cyclotron Laboratory, Michigan State University, for providing the computer code OXBASH.

References

1. Tanihata I., Hamagaki H., Hashimoto O., Shida Y., Yoshikawa N., Sugimoto K., Yamakawa O., and Kobayashi T. **1985**. Measurement of interaction cross sections and nuclear radii in the light p-shell region. *Physical Review Letters*, **55**(24), pp: 2676-2679.
2. Tanihata I., Hamagaki H., Hashimoto O., Nagamiya S., Shida Y., Yoshikawa N., Yamakawa O., Sugimoto K., Kobayashi T., Greiner D. E., Takahashi N. and Nojiri Y. **1985**. Measurement of interaction cross sections and radii of He isotopes. *Physics Letters B*, **160**(6), pp: 380-384.
3. Hansen P. G. and Jonson B. **1987**. The neutron halo of extremely neutron-rich nuclei. *Europhysics Letters*, **4**(4), pp: 409-414.
4. Tanihata I., Kobayashi T., Yamakawa O., Shimoura S., Ekuni K., Sugimoto K., Takahashi N., Shimoda T. and Sato H. **1988**, Measurement of interaction cross sections using isotope beams of Be and B and isospin dependence of nuclear radii. *Physics Letters B*, **206**(4), pp: 592-596.
5. Zukov M. V., Danilin B. V., Fedorov D. V., Bang J. M., Thompson I. J. and Vaagen J. S. **1993**. Bound state properties of Borromean halo nuclei: ${}^6\text{He}$ and ${}^{11}\text{Li}$. *Physics Reports*. **231**(4), pp: 151-199.
6. Al-Khalili J. S., Tostevin J. A. and Thompson I. J. **1996**. Radii of halo nuclei from cross section measurements. *Physical Review C*. **54**(4), pp: 1843-1852.
7. Technical Proposal for the Design, Construction, Commissioning, and Operation of the ELISe setup, Haik Simon, GSI Internal Report, Dec. (2005)
8. Suda T. and Wakasugi M. **2005**. Structure studies of unstable nuclei by electron scattering. *Progress in Particle and Nuclear Physics*. **55**, pp: 417-436.
9. Ozawa A., Bochkarev O., Chulkov L., Cortina D., Geissel H. H., Hellstrom M., Ivanov M., Janik R., Kimura K., Kobayashi T., Korshennikov A. A., Munzenberg G., Nickel F., Ogawa Y., Ogloblin A. A., Pfitzner M., Pribora V., Simon H., Sitar B., Strmen P., Summerer K., Suzuki T., Tanihata I., Winkler M. and Yoshida K. **2001**. Measurements of interaction cross sections for light neutron-rich nuclei at relativistic energies and determination of effective matter radii. *Nuclear Physics A*. **691**, pp: 599-617.
10. Yoshiko Kanada-EN'YO and Hisashi Horiuchi. **16 Jul 2001**. Structure of light untable nuclei studied with antisymmetrized molecular dynamics. arXiv: nucl-th/0107044v1, pp: 1-72.
11. Maddalena V., Aumann T., Bazin D., Brown B. A., Caggiano J. A., Davids B., Glasmacher T., Hansen P. G., Ibbotson R. W., Navin A., Pritychenko B. V., Scheit H., Sherrill B. M., Steiner M., Tostevin J. A., and Yurkon J. **2001**. Single-nucleon knockout reactions: Application to the spectroscopy of ${}^{16,17,19}\text{C}$. *Physical Review C*. **63**(024613), pp: 1-17.
12. Toshio Suzuki, Hiroyuki Sagawa and Kouichi Hagino. **2003**. Electromagnetic moments and electric dipole transitions in carbon isotopes. *Physical Review C*. **68**(014317), pp: 1-10.
13. Sagawa H., Zhou X. R., Zhang X. Z. and Toshio Suzuki. **2004**. Deformation and electromagnetic moments in carbon and neon isotopes. *Physical Review C*. **70**(054316), pp: 1-14.
14. Dao T. Khoa, Hoang Sy Than, Tran Hoai Nam, Marcella Grasso, and Nguyen Van Giai. **2004**. Microscopic calculation of the interaction cross section for stable and unstable nuclei based on the nonrelativistic nucleon-nucleon t matrix. *Physical Review C*. **69**(044605), pp: 1-12.
15. Horiuchi W. and Suzuki Y. **2006**. ${}^{22}\text{C}$: An s-wave two-neutron halo nucleus. *Physical Review C*. **74** (034311), pp: 1-5.

16. Abu-Ibrahim B., Horiuchi W., Kohama A., and Suzuki Y. **2008**. Reaction cross sections of carbon isotopes incident on a proton. *Physical Review C*. **77** (034607),pp: 1-11.
17. Chen Yu, Zhang Feng-Shou and Su Jun. **2009**. A Discussion on whether $^{15-20}\text{C}$ are all skin nuclei via isospin-dependent Boltzmann-Langevin equation. *Chinese Physics Letter*. **26**(11),pp: 1-4.
18. Simpson E. C. and Tostevin J. A. **2009**. One- and two-neutron removal from the neutron-rich carbon isotopes. *Physical Review C*. **79** (024616),pp: 1-10.
19. Panda R. N. and Patra S. K. **24 Oct 2010**. Structure effect on one neutron removal reaction using relativistic mean field densities in Glauber model. arXiv: nucl-th/1010.4938v1.
20. Navratil P. and Barrett B. R. **1996**. No-core shell-model calculations with starting-energy-independent multivalued effective interactions. *Physical Review C*. **54**(6),pp: 2986-2995.
21. Navratil P. and Barrett B. R. **1998**. Large-basis shell-model calculations for p-shell nuclei. *Physical Review C*. **57** (6),pp: 3119-3128.
22. Caurier E. and Navratil P. **2006**. Proton radii of 4,6,8He isotopes from high-precision nucleon-nucleon interactions. *Physical Review C*. **73**(021302(R)),pp: 1-5.
23. Karataglidis S., Amos K., Fraser P., Canton L. and Svenne J. P. **2008**. Constraints on the spectra of $^{17,19}\text{C}$. *Nuclear Physics A*. **813**,pp: 235-251.
24. Kuo T. T. S., Muether H. and Amir-Azimi-Nili K. **1996**. Realistic effective interactions for halo nuclei. *Nuclear Physics A*. **606**,pp: 15-26.
25. Kuo T. T. S., Krmpotic F. and Tzeng Y. **1997**. Suppression of core polarization in halo nuclei. *Physical Review Letters*. **78**(14),pp:2708-2711.
26. Brown B. A., Radhi R. and Wildenthal B. H. **1983**. Electric quadrupole and hexadecupole nuclear excitations from the perspectives of electron scattering and modern shell-model theory. *Physics Reports*. **101**(5),pp: 313-358.
27. Warburton E. K. and Brown B. A. **1992**. Effective interactions for the $0p_{1/2}0d$ nuclear shell-model space. *Physical Review C*. **46**(3),pp: 923-944.
28. R. A. Radhi, **1983**. Calculations of elastic and inelastic electron scattering in light nuclei with shell-model wave functions. Ph.D.Thesis. Department of Physics, Michigan State University, USA. p.11.
29. Brown B. A., Etchegoyen A., Godwin N. S., Rae W. D. M., Richter W. A., Ormand W. E., Warburton E. K., Winfield J. S., Zhao L. and Zimmerman C. H. **2005**. Oxbash for Windows PC. MSU-NSCL report number 1289.
30. Heisenberg J., McCarthy J. S. and Sick I. **1970**. Elastic electron scattering from ^{13}C . *Nuclear Physics A*. **157**,pp: 435-448.
31. Sick I. and McCarthy J. S. **1970**. Elastic electron scattering from ^{12}C and ^{16}O . *Nuclear Physics A*. **150**,pp: 631-654.
32. Li G. C., Yearian M. R. and Sick I. **1974**. High-momentum-transfer electron scattering from ^{24}Mg , ^{27}Al , ^{28}Si , and ^{32}S . *Physical Review C*. **9**(5),pp: 1861-1877.